Superconducting proximity effect and zero-bias anomaly in transport through quantum dots weakly attached to ferromagnetic leads

Ireneusz Weymann* and Piotr Trocha
Faculty of Physics, Adam Mickiewicz University, 61-614 Poznań, Poland
(Received 29 October 2013; revised manuscript received 30 January 2014; published 10 March 2014)

The Andreev transport through a quantum dot coupled to two external ferromagnetic leads and one superconducting lead is studied theoretically by means of the real-time diagrammatic technique in sequential and cotunneling regimes. We show that the tunnel magnetoresistance (TMR) of the Andreev current displays a nontrivial dependence on the bias voltage and the level detuning and can be described by analytical formulas in the zero-temperature limit. The cotunneling processes lead to a strong modification of the TMR, which is most visible in the Coulomb blockade regime. We find a zero-bias anomaly of the Andreev differential conductance in the parallel configuration, which is associated with a nonequilibrium spin accumulation in the dot triggered by Andreev processes.

DOI: 10.1103/PhysRevB.89.115305 PACS number(s): 72.25.Mk, 74.45.+c, 73.23.Hk, 85.35.Be

I. INTRODUCTION

The large tunability of quantum dot properties by application of proper gate voltages makes these structures very promising for spintronic and quantum information applications [1,2]. These nanoscale structures enable the observation of various novel phenomena and exhibit effects known from solid-state physics, atomic physics, or quantum optics [3]. Moreover, nanoscopic systems with quantum dots coupled to ferromagnetic leads can exhibit a considerable tunnel magnetoresistance (TMR) effect and can be used for spin current generation [4–8]. Theoretical and experimental investigations of transport through such structures are thus of great current interest. Transport properties of single quantum dots attached to ferromagnetic leads have been extensively investigated both experimentally [9–16] and theoretically [17–20]. The physics, however, becomes much more interesting and fascinating when these nanostructures are in proximity to a superconductor. In such hybrid structures, transport properties are determined by the interplay of the spin-dependent tunneling and superconducting correlations [21].

Hybrid nanoscopic structures consisting of quantum dots attached to normal and superconducting external leads have attracted great interest, mainly due to the possibility of creation of nonlocal entangled electron pairs [22,23]. The generation of entangled pairs is strictly connected with the processes known as crossed Andreev reflections (CARs). In contrast to the usual Andreev reflection, in CAR the hole is reflected back into the electrode, which is spatially separated from the lead, from which the incoming electron arrives. Such processes have been investigated both theoretically and experimentally in hybrid metallic structures [24–26]. Moreover, a very recently more efficient and easy tunable Cooper-pair beam splitter has been implemented by using double-quantum-dot structures [22,23]. Quantum dots thus provide an interesting and promising route for manipulating entangled electrons by electrical means in a controllable fashion, which no doubt is of great importance for quantum computation and quantum information [1]. However, to exploit them efficiently and reliably, it is crucial to understand various properties of such hybrid nanostructures, including transport properties due to Andreev reflection.

In this paper, we therefore investigate the Andreev transport through single-level quantum dots, with special focus on the interplay of the spin-dependent and Andreev tunneling processes. For this, we assume that the dot is coupled to two ferromagnetic leads and one *s*-wave superconducting electrode, where the coupling to ferromagnets is weak, while the coupling to the superconductor can be arbitrary. We assume that the magnetic moments of the ferromagnetic leads may be aligned either in parallel or antiparallel. The difference in these two magnetic configurations gives rise to the TMR of the Andreev current. Since the amount of CAR is affected by changes in the magnetic configuration, by studying the behavior of the TMR one can obtain information about the role of CARs in transport. We note that transport properties of hybrid systems consisting of quantum dots coupled to ferromagnetic and superconducting electrodes have already been studied. The considerations, however, concerned the case of one ferromagnetic and one superconducting lead [21,27–30]. In such geometry, CARs are not allowed. On the other hand, CAR was studied in the case of two normal leads and one superconducting lead in the absence of intradot Coulomb interactions [31,32]. Nevertheless, the Coulomb interactions, which are strong in typical quantum dots, may weaken the proximity effect induced on the dot or even completely destroy it [33,34]. Thus, the effects of Coulomb correlations should be regarded on an equal footing with the other effects, such as, e.g., superconducting correlations, nonequilibrium, and the magnetism of the leads. Moreover, the case when the normal leads are replaced by ferromagnets was studied theoretically, but only in the sequential tunneling regime [33,34]. The sequential tunneling approximation may, however, lead to incorrect predictions, especially for the TMR in the Coulomb blockade regime [20]. The goal of the present work is thus to extend theses studies, by calculating the Andreev transport for realistic quantum dot parameters, including both sequential and cotunneling processes.

To calculate the basic transport characteristics, in both equilibrium and nonequilibrium, we employ the real-time diagrammatic technique [35]. Particularly, by taking into account the first- and second-order diagrams, we calculate

*weymann@amu.edu.pl

the Andreev current, differential conductance, and TMR. We discuss the influence of cotunneling processes on the sequential Andreev transport, which has been studied in Refs. [33] and [34], and show that it leads to a strong modification of the TMR for bias voltages where the Andreev current is suppressed due to the charging effects. Moreover, we predict a zero-bias anomaly in the differential conductance of the Andreev current for the parallel magnetic configuration of the device, which is due to the nonequilibrium spin accumulation in the dot induced by cotunneling processes.

The paper is organized as follows. In Sec. II we describe the model and method used in calculations. Section III is devoted to numerical results and their discussion. We first analyze the dependence of the Andreev current and differential conductance on the bias voltage and the detuning of the dot level and then discuss the behavior of the associated TMR. We also analyze the behavior of the zero-bias anomaly for various model parameters. Finally, the conclusions are given in Sec. IV.

II. THEORETICAL DESCRIPTION

A. Model Hamiltonian

We consider a single-level quantum dot tunnel coupled to two ferromagnetic leads and one superconducting electrode, as shown schematically in Fig. 1. The magnetizations of the leads are assumed to be collinear, and the system can be either in the parallel or the antiparallel magnetic configuration. The magnetic configuration of the system can be switched by applying a weak external magnetic field. Since there is also a superconducting electrode attached to the dot, the magnetic field that switches the orientations of the magnetizations of ferromagnetic leads needs to be smaller than the corresponding critical magnetic field of the superconductor. The Hamiltonian of the system acquires the form

$$H = \sum_{\beta=L,R} H_\beta + H_S + H_{\rm QD} + H_T, \tag{1}$$

where the first term, H_β, describes the left ($\beta = L$) and right ($\beta = R$) electrodes in the noninteracting quasiparticle approximation, $H_\beta = \sum_{\mathbf{k}\sigma} \varepsilon_{\mathbf{k}\beta\sigma} c^\dagger_{\mathbf{k}\beta\sigma} c_{\mathbf{k}\beta\sigma}$. Here, $c^\dagger_{\mathbf{k}\beta\sigma}$ ($c_{\mathbf{k}\beta\sigma}$) is the creation (annihilation) operator of an electron with the wave vector $\mathbf{k}$ and spin σ in the lead β, whereas $\varepsilon_{\mathbf{k}\beta\sigma}$ denotes the corresponding single-particle energy. The second term in Eq. (1) describes the s-wave BCS superconducting lead in the mean-field approximation,

$$H_S = \sum_{\mathbf{k}} \sum_{\sigma} \varepsilon_{\mathbf{k}S\sigma} c^\dagger_{\mathbf{k}S\sigma} c_{\mathbf{k}S\sigma} + \sum_{\mathbf{k}} (\Delta^* c_{\mathbf{k}S\downarrow} c_{-\mathbf{k}S\uparrow} + \Delta c^\dagger_{-\mathbf{k}S\uparrow} c^\dagger_{\mathbf{k}S\downarrow}), \tag{2}$$

with $\varepsilon_{\mathbf{k}S\sigma}$ denoting the relevant single-particle energy and Δ being the order parameter of the superconductor. Without loss of generality, the order parameter can be chosen real and positive, $\Delta = |\Delta|$. The third term in Hamiltonian (1) describes the single-level quantum dot and has the form

$$H_{\rm QD} = \sum_{\sigma} \varepsilon d^\dagger_\sigma d_\sigma + U n_\uparrow n_\downarrow, \tag{3}$$

where ε denotes the dot's level energy and U is the corresponding Coulomb repulsion energy.

Finally, the tunneling of electrons between all the leads (L, R, S) and the quantum dot can be modeled by the Hamiltonian

$$H_T = \sum_{\mathbf{k}\sigma} \sum_{\beta=L,R,S} \left(V^\beta_{\mathbf{k}\sigma} c^\dagger_{\mathbf{k}\beta\sigma} d_\sigma + \text{h.c.} \right), \tag{4}$$

with $V^\beta_{\mathbf{k}\sigma}$ denoting the relevant tunneling matrix elements. In the following we assume that these matrix elements are $\mathbf{k}$ and σ independent. The coupling of the dot to the ferromagnetic lead ($\beta = L, R$) can be parametrized by $\Gamma^\sigma_\beta = 2\pi |V^\beta|^2 \rho^\sigma_\beta$, where ρ^σ_β is the density of states of lead β for spin σ. Within the wide band approximation the couplings become energy independent and constant. By introducing the spin polarization of lead β, $p_\beta = (\rho^+_\beta - \rho^-_\beta)/(\rho^+_\beta + \rho^-_\beta)$, the couplings can be written in the form, $\Gamma^\sigma_L = \Gamma_L(1 + \tilde{\sigma} p)$ and $\Gamma^\sigma_R = \Gamma_R(1 \pm \tilde{\sigma} p)$, with $\tilde{\sigma} = 1$ for $\sigma = \uparrow$, $\tilde{\sigma} = -1$ for $\sigma = \downarrow$, and the upper (lower) sign in Γ^σ_R corresponding to the parallel (antiparallel) magnetic configuration.

As we are interested in the Andreev transport regime, in our considerations we can take the limit of an infinite superconducting gap, $\Delta \to \infty$. Then the quantum dot coupled to the superconducting lead can be described by the following effective Hamiltonian [36]:

$$H^{\rm eff}_{\rm QD} = H_{\rm QD} - \frac{\Gamma_S}{2} d^\dagger_\uparrow d^\dagger_\downarrow - \frac{\Gamma_S}{2} d_\downarrow d_\uparrow. \tag{5}$$

It can be clearly seen that the superconducting proximity effects are included in the last two terms in Eq. (5), where the effective pair potential Γ_S is the coupling strength between the

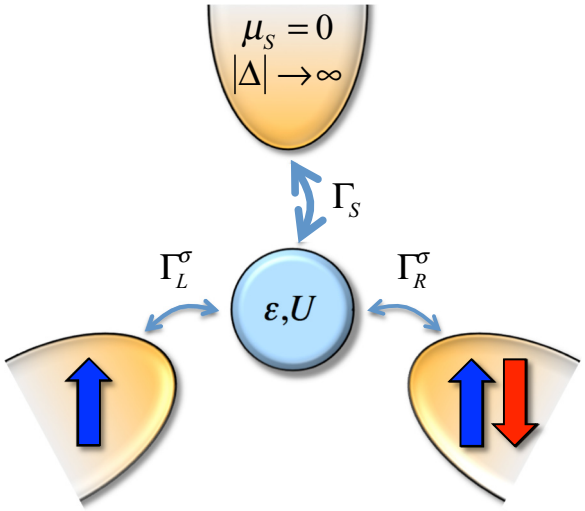

FIG. 1. (Color online) Schematic of a quantum dot strongly coupled to an s-wave superconductor and weakly coupled to two ferromagnetic leads. The coupling to the superconductor is described by Γ_S, while the spin-dependent couplings to ferromagnetic leads are denoted Γ^σ_L and Γ^σ_R, respectively. Magnetizations of the ferromagnets can form either a parallel or an antiparallel magnetic configuration, as indicated. The superconducting gap Δ is assumed to be the largest energy scale in the problem, $|\Delta| \to \infty$, and the electrochemical potential of the superconducting lead is set to 0, $\mu_S = 0$. ε denotes the dot level energy and U is the Coulomb repulsion on the dot.

dot and the superconducting electrode and acquires the form $\Gamma_S = 2\pi|V^S|^2\rho_S$. Here, ρ_S denotes the density of states of the superconductor in the normal state, whereas V^S is the relevant tunnel amplitude between the dot and the superconducting electrode.

The eigenstates of the effective dot's Hamiltonian, (5), can be easily found to be the singly occupied dot $|\sigma\rangle$, with either spin-up or spin-down, and the two states being the superpositions of the empty $|0\rangle$ and doubly occupied $|2\rangle$ states:

$$|\pm\rangle = \frac{1}{\sqrt{2}}\left(\sqrt{1 \mp \frac{\delta}{2\varepsilon_A}}\,|0\rangle \mp \sqrt{1 \pm \frac{\delta}{2\varepsilon_A}}\,|2\rangle\right). \tag{6}$$

The corresponding eigenenergies are $E_\uparrow = E_\downarrow = \varepsilon$ and $E_\pm = \delta/2 \pm \varepsilon_A$, where $\delta = 2\varepsilon + U$ denotes the detuning from the particle-hole symmetry point, whereas $\varepsilon_A = \sqrt{\delta^2 + \Gamma_S^2}/2$ measures the energy difference between state $|+\rangle$ and state $|-\rangle$.

The Andreev bound-state energies can be defined as excitation energies of the effective dot Hamiltonian [34],

$$E^A_{\alpha\beta} = \alpha\frac{U}{2} + \frac{\beta}{2}\sqrt{\delta^2 + \Gamma_S^2}, \tag{7}$$

where $\alpha,\beta = \pm$. These energies are defined by differences between the eigenenergies of the dot decoupled from the ferromagnetic leads. E_{++} (E_{+-}) denotes the excitation from the singly occupied state $|\sigma\rangle$ to state $|+\rangle$ ($|-\rangle$), while the excitation energies E_{--} and E_{-+} are related with the opposite transitions.

We would like to note that by using the effective Hamiltonian, (5), we assumed that Δ is the largest energy scale in the problem, which implies that $\Delta > U$. Clearly, this condition may not be fulfilled in any hybrid device with a quantum dot coupled to a superconducting lead. However, there are superconductors [37,38] in which the energy gap can be as large as a couple of milli–electron volts, while the charging energy in quantum dots depends on their size and can be made arbitrarily low. Here, however, one needs to balance between the charging and the thermal energies, so that the finite-size and charging effects are not smeared out by thermal fluctuations. Consequently, the experimental implementation of hybrid quantum dots where the condition $\Delta > U$ is fulfilled is feasible.

B. Calculation method

To calculate the transport characteristics of the considered system we employ the real-time diagrammatic technique [35], adopted for the case with a superconducting lead [39,40]. The technique is based on the perturbation expansion of the reduced density matrix and the relevant operators with respect to the coupling strength to ferromagnetic leads. After integrating out the noninteracting electronic degrees of freedom in the ferromagnetic leads, the system is described by reduced density matrix $\hat{\rho}$, which, in the steady state, is governed by the equation [35]

$$\sum_{\chi'} \Sigma_{\chi,\chi'} P_{\chi'} = 0, \tag{8}$$

where P_χ denotes an element of the reduced density matrix, $P_\chi = \langle\chi|\hat{\rho}|\chi\rangle$, taken in the dot's state $|\chi\rangle$, whereas $\Sigma_{\chi,\chi'}$ are the self-energies corresponding to the evolution forward in time from state $|\chi'\rangle$ to state $|\chi\rangle$ and then backward in time from state $|\chi\rangle$ to state $|\chi'\rangle$. Note that Eq. (8) describes only diagonal elements of the reduced density matrix. Generally, off-diagonal elements corresponding to coherent superpositions of states $|+\rangle$ and $|-\rangle$ should also be considered. However, in the case of $\Gamma_\beta \ll \Gamma_S$ ($\beta = L,R$), as considered in this paper, the transition rates between state $|+\rangle$ and state $|-\rangle$ become irrelevant and can thus be neglected [34]. The diagonal elements of the reduced density matrix, P_χ, simply denote the probability of finding the dot (in the proximity with superconductor) in state $|\chi\rangle$. The current flowing from the ferromagnetic β lead can be calculated from the formula [35]

$$I_\beta = -\frac{ie}{\hbar}\sum_{\chi,\chi'} \Sigma^{I_\beta}_{\chi,\chi'} P_{\chi'} \tag{9}$$

for $\beta = L,R$. Here, $\Sigma^{I_\beta}_{\chi,\chi'}$ denotes the generalized self-energy, which takes into account the number of electrons transferred through a given junction β.

In the weak-coupling regime, $\Gamma_\beta \ll k_BT$, Eq. (8) can be solved order by order in the perturbation expansion in the coupling strength to ferromagnetic leads. Each term of expansion can be visualized graphically as a diagram (or sum of diagrams) defined on the Keldysh contour, where the vertices are connected by lines corresponding to tunneling processes. The self-energies in respective order of expansion can be calculated using the respective diagrammatic rules [34,41]. Having determined the respective self-energies and occupation probabilities, the current can then be calculated in a given order of expansion. Here, we have calculated the relevant contributions up to the second order of expansion [41]. The first order of expansion corresponds to sequential tunneling processes, which dominate the current for voltages higher than a threshold voltage. Below the threshold, however, the sequential tunneling is exponentially suppressed due to the charging energy and the system is in the Coulomb blockade regime. In the Coulomb blockade regime transport is dominated by cotunneling processes, which involve two correlated-in-time single tunneling events occurring through virtual states of the system [42]. These processes are captured by the second order of expansion. Note that in the hybrid device considered here, these processes are also related to transferring Cooper pairs between the ferromagnets and the superconductor.

Due to the proximity of the superconducting lead and Andreev processes between the dot and the superconductor, the currents flowing through the left and right junctions are generally not equal, $I_L \neq I_R$. The total current flowing into the superconductor can thus be simply obtained from Kirchhoff's law:

$$I_S = I_L + I_R. \tag{10}$$

III. RESULTS AND DISCUSSION

In this section we present the numerical results for Andreev transport through quantum dots in the limit of a large superconducting gap. Particularly, we show the charge current

injected (extracted) into (from) the superconducting lead and the corresponding differential conductance. We also calculate the TMR effect associated with the change of magnetic configuration of the ferromagnetic leads from the parallel to the antiparallel alignment. The latter quantity is defined as the ratio

$$\mathrm{TMR} = \frac{I_S^{\mathrm{AP}} - I_S^{\mathrm{P}}}{I_S^{\mathrm{P}}}, \tag{11}$$

where I_S^{P} and I_S^{AP} denote the Andreev current flowing into the superconductor in the parallel and antiparallel magnetic configurations, respectively.

For the three-terminal setup considered in this paper, the TMR can be used to quantify the role of CAR, compared to direct Andreev reflection (DAR) [33]. The rate of a direct Andreev process is proportional to the product of the coupling constants for spin-up and spin-down of the same junction. This is contrary to CAR, the rate of which is proportional to the product of respective couplings, but for different leads. Thus, any change in the magnetic configuration leads to a change in CAR, while direct Andreev processes are not affected. Consequently, the TMR provides the relevant, though indirect, information about CAR in the system, since any change in TMR is related to a change in CAR. In an extreme situation when the leads become half-metallic, only CARs are possible. The current is then maximized in the antiparallel configuration and completely suppressed in the parallel one.

In the numerical analysis we assume that the system is symmetric, i.e., $\Gamma_L = \Gamma_R = \Gamma/2$ and $p_L = p_R = p$. We also assume that the voltage drop is applied symmetrically between the magnetic leads and the superconductor, $\mu_L = \mu_R = eV$ and $\mu_S = 0$. For this configuration of applied voltages, the effect of the left-right contact asymmetry is rather intuitive, as it mainly leads to quantitative changes. For example, increasing the spin polarization of one lead generally boosts the TMR by a certain factor, while its bias and gate voltage dependence qualitatively almost do not change. In our analysis we also assume that the external magnetic field B_z required to switch the magnetic configuration of the system from parallel to antiparallel, and vice versa, is so small that it does not lead to splitting of the dot level, i.e., $B_z \ll \Gamma$.

A. Andreev current and differential conductance

When applying a negative bias voltage, $eV > 0$ (note that $e < 0$), one injects pairs of electrons into the superconductor, whereas for a positive bias, $eV < 0$, the Cooper pairs tunnel to ferromagnetic leads. If the two electrons coming from the same lead enter the superconductor as a Cooper pair, this process is called DAR. In turn, CAR occurs when the electrons leaving from spatially separated ferromagnetic leads are injected into the superconductor. For negative bias voltages inverse processes take place. Particularly, a Cooper pair leaving the superconductor can tunnel to the same ferromagnetic electrode (DAR) or split into entangled electrons injected into separate leads (CAR).

In the considered system the current flowing for a negative electrochemical potential shift, $eV < 0$, is related to the current flowing for $eV > 0$ by making the transformation $eV \to -eV$, $\delta \to -\delta$, and $I_S \to -I_S$. Thus, it is generally

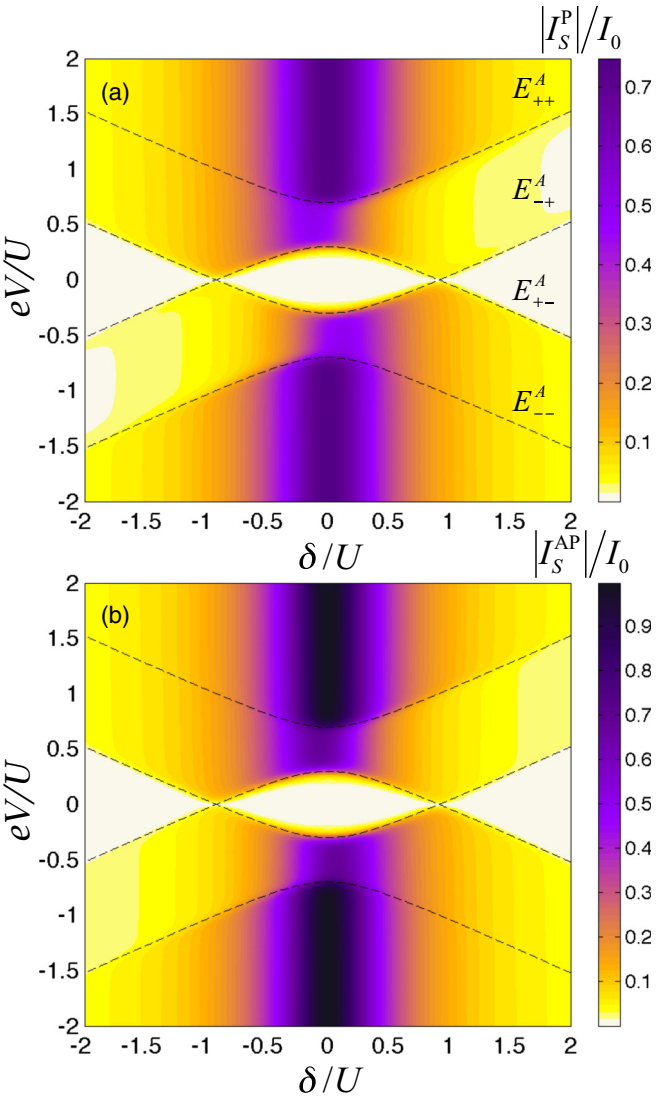

FIG. 2. (Color online) Absolute value of the total Andreev current for (a) the parallel (I_S^{P}) and (b) the antiparallel (I_S^{AP}) magnetic configuration as a function of the detuning $\delta = 2\varepsilon + U$ and applied bias voltage V. Dashed lines indicate the position of the respective Andreev bound states [see Eq. (7)] as denoted in (a). Parameters are $\Gamma_S = 0.4$, $\Gamma = 0.01$, and $T = 0.02$, with $U \equiv 1$ the energy unit, and $p = 0.5$. The current is plotted in units of $I_0 = e\Gamma/\hbar$. The same color scale is used in (a) and (b) to enable direct comparison.

sufficient to consider the case of only one bias polarization. Before analyzing the magnetoresistive properties of our hybrid device, let us first discuss the general behavior of the Andreev current depending on the transport region. The bias voltage eV and detuning $\delta = 2\varepsilon + U$ dependence of the absolute value of the total current flowing between the superconducting and the ferromagnetic leads is shown in Fig. 2 for the parallel and antiparallel magnetic configurations. First, one can see that the Andreev current becomes significant only for small values of the detuning parameter δ. This is due to the fact that the Andreev tunneling is optimized when the particle-hole symmetry holds, i.e., in the case of $\delta \to 0$. Furthermore, the Andreev current vanishes for low bias voltages, $E^A_{-+} < eV <$

E^A_{+-}, and for $|\delta| < \sqrt{U^2 - \Gamma_S^2}$, when the dot is occupied by a single electron. As two electrons are required to form a Cooper pair, no current is flowing into the superconductor. For $|\delta| = \sqrt{U^2 - \Gamma_S^2}$, i.e., the point at which the two levels E^A_{+-} and E^A_{-+} cross each other [see Fig. 2(a)], the Andreev current vanishes only for zero bias voltage. In turn, for $|\delta| > \sqrt{U^2 - \Gamma_S^2}$, the current is suppressed for a finite region of low bias voltage, namely, that which corresponds to an empty or doubly occupied dot regime. The Andreev current starts to flow when the chemical potentials of ferromagnetic leads cross the Andreev bound-state energies E^A_{+-} or E^A_{-+}. The current increases again when the next Andreev levels E^A_{++} or E^A_{--} enter the bias window (see Fig. 2).

The above-described behavior is also clearly visible in the dependence of the differential conductance on the bias voltage eV and the detuning parameter δ, which is shown in Fig. 3. Each time the electrochemical potential of ferromagnetic leads eV meets the Andreev level, a peak appears in the differential conductance. Generally, the bias voltage dependence of the differential conductance reveals four peaks, except for the values of detuning $\delta = \pm\sqrt{U^2 - \Gamma_S^2}$, for which states E^A_{+-} and E^A_{-+} become degenerate (see Fig. 3 for $\delta \approx \pm U$). Furthermore, the behavior of the transport characteristics is asymmetric with respect to the bias reversal, which is nicely visible in the differential conductance. More specifically, the magnitude of the peak associated with the Andreev level E^A_{++} for $eV > 0$ and $\delta > 0$ is larger than the amplitude of the corresponding level E^A_{--} for $eV < 0$ (and $\delta > 0$). A similar asymmetry can be observed for the same Andreev states, but for opposite detuning, $\delta < 0$. The reason for this asymmetric behavior of the Andreev current can be understood as follows. Let us consider the asymmetry occurring for large positive values of δ. In this case the energies ε and $\varepsilon + U$ lie above the chemical potential of the superconducting lead and the dot is empty. When shifting the electrochemical potentials of ferromagnetic leads down, $eV < 0$, there are no states in the transport window and the tunneling rate of Cooper pairs into superconductor becomes strongly suppressed. However, it is sufficient to change either the sign of the bias voltage V or the sign of the detuning δ to allow for Andreev tunneling. This leads to a highly asymmetric dependence of the differential conductance on the bias voltage and detuning, which is visible in both the parallel and the antiparallel magnetic configurations of the device (see Fig. 3).

The Andreev current flows due to both direct and crossed Andreev processes. To quantify the role of these processes, one can use ferromagnetic contacts and, by introducing the spin dependence of tunneling processes, study how the current and differential conductance depend on the magnetic configuration of the device [33]. The presence of CAR reveals itself just in the dependence of the Andreev current on the magnetic configuration. More specifically, in the antiparallel configuration both electrons forming a Cooper pair belong to either the majority or the minority bands of the ferromagnets. On the other hand, in the parallel configuration one of the electrons is always a majority one, while the other is a minority one. The conductance is then determined by the minority spin band of the ferromagnet. The current flowing in the parallel magnetic configuration is therefore suppressed compared to the current flowing in the antiparallel configuration. This can be clearly seen in the bias voltage and detuning dependence of both the current (see Fig. 2) and the differential conductance (see Fig. 3). Note that this behavior is just opposite to the typical quantum dot spin valves, where usually the conductance in the parallel configuration is higher than that in the antiparallel configuration [17,18,20].

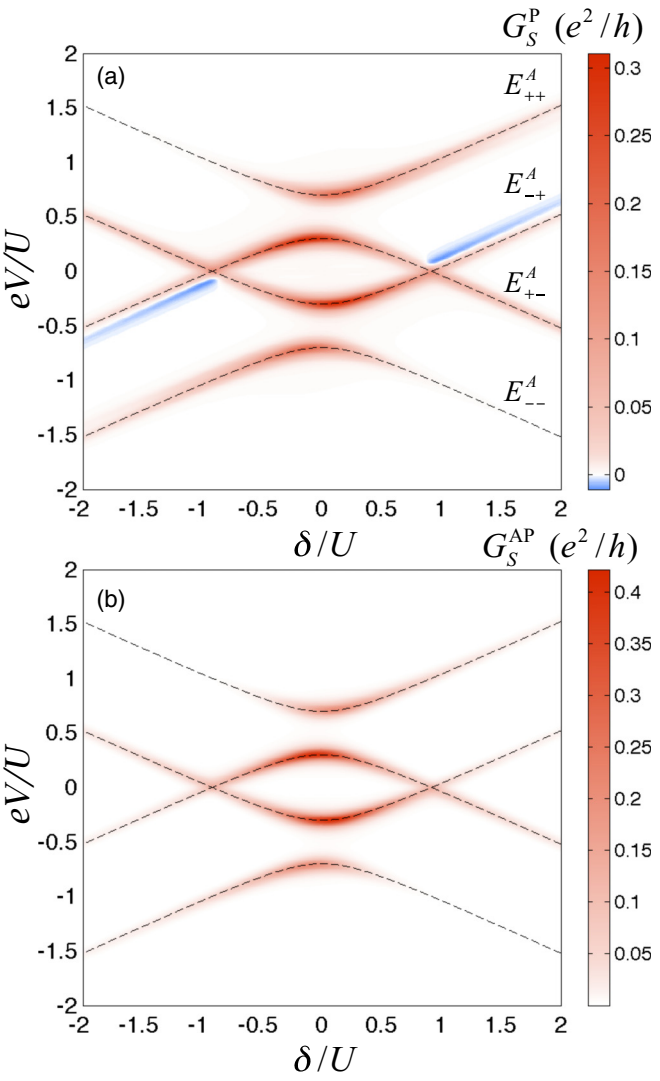

FIG. 3. (Color online) Total differential conductance $G_S = dI_S/dV$ due to the Andreev current for (a) the parallel (G_S^{P}) and (b) the antiparallel (G_S^{AP}) magnetic configuration as a function of the detuning $\delta = 2\varepsilon + U$ and applied bias voltage V. Dashed lines indicate the position of the respective Andreev bound states. Parameters are as in Fig. 2.

Moreover, the differential conductance calculated for the parallel alignment reveals another interesting feature. For $|\delta| > \sqrt{U^2 - \Gamma_S^2}$, some negative values of the differential conductance appear in the vicinity of E^A_{-+} (E^A_{+-}) for a positive (negative) electrochemical potential shift [see Fig. 3(a)]. This can be understood by realizing that in the parallel configuration there are more spin-up electrons than spin-down ones at

the Fermi level of ferromagnetic leads. Since injecting (or extracting) a Cooper pair to the superconductor involves two spins of opposite directions, the rate of electron pairs is mainly determined by the density of states of minority carriers, which is the bottleneck for Andreev transport in the parallel configuration. Such a spin imbalance leads to the nonequilibrium spin accumulation in the dot that develops when the dot occupancy is odd. The occupation of the spin-up level then becomes greatly enhanced compared to that of the spin-down level (the situation can be reversed by applying the opposite bias voltage), suppressing the Andreev current and giving rise to negative differential conductance. Upon a further increase in the bias voltage, the occupancy of the dot changes to even (for $|eV| \approx E^A_{++}$ or $|eV| \approx E^A_{--}$) and the dependence on the spin is weakened. Consequently, no negative differential conductance occurs then. On the other hand, for $|\delta| < \sqrt{U^2 - \Gamma_S^2}$ and a low bias voltage, the dot is in the Coulomb blockade regime and the Andreev current is generally suppressed. Upon reaching the threshold voltage, the singlet states of the dot start to participate in transport and the current changes monotonically. We also note that for the antiparallel magnetic configuration no negative differential conductance occurs, since in this case both electrons forming a Cooper pair belong to the same subband of the ferromagnets and there is no spin accumulation.

B. Tunnel magnetoresistance

As mentioned above, the presence of crossed Andreev processes can be revealed by studying the change in transport properties when the magnetic configuration of the device is varied. In this section we therefore analyze the behavior of the TMR on the bias voltage and the detuning parameter δ. Figure 4 presents both the total TMR and the TMR calculated using only the first-order tunneling processes [$\mathrm{TMR}^{(1)}$]. In addition, in Figs. 5 and 6 we show the bias voltage dependence of the current, differential conductance, and TMR for two values of detuning δ, for which the effect of second-order processes is most visible. It is clearly visible that cotunneling processes introduce qualitative differences in the behavior of the TMR, compared to the TMR obtained considering only first-order processes. First, it is shown that the sequential TMR is positive in the whole transport regime [see Fig. 4(a)], while the total TMR exhibits negative values for low bias voltages and in the range of detuning parameter $|\delta| < \sqrt{U^2 - \Gamma_S^2}$ [see Fig. 4(b)]. Second, for $|\delta| > \sqrt{U^2 - \Gamma_S^2}$ and for bias voltages $E^A_{+-} < eV < E^A_{-+}$, the total TMR becomes finite, while the sequential TMR is much suppressed. To explain the behavior of the TMR on the transport regime, let us now discuss the relevant cross sections of the density plots shown in Fig. 4.

In Fig. 5 we plot the bias dependence of the current [Fig. 5(a)], the differential conductance [Fig. 5(b)] for parallel and antiparallel configurations, and the TMR effect [Fig. 5(c)] for detuning $\delta/U = 2$. As described above, the voltage dependence reveals asymmetry with respect to the bias reversal. There are three steps in the Andreev current as a function of the bias voltage, which correspond to the respective Andreev peaks in the differential conductance [see Figs. 5(a) and 5(b)].

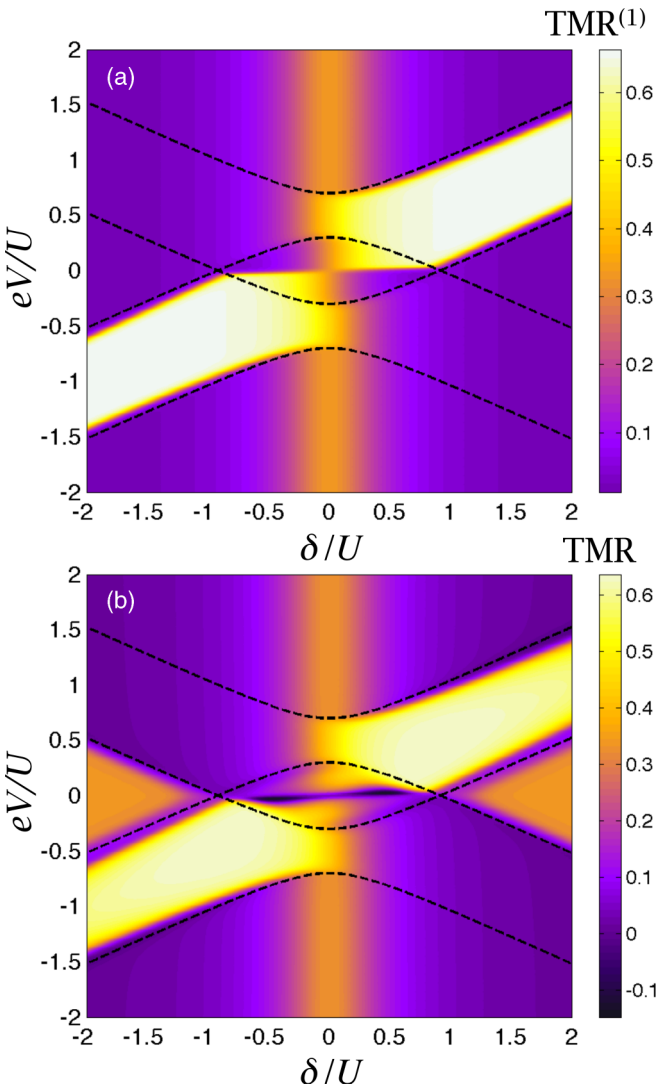

FIG. 4. (Color online) The tunnel magnetoresistance (TMR) of the Andreev current as a function of the detuning δ and the bias voltage V calculated by using only (a) sequential tunneling processes [$\mathrm{TMR}^{(1)}$] and (b) the first- and second-order tunneling processes. Parameters are the same as in Fig. 2. Dashed lines show the position of Andreev bound states. The same color scale is used in (a) and (b) to facilitate comparison.

One can also note the regime of suppressed current in the parallel configuration visible for $U/2 \lesssim eV \lesssim 3U/2$ and the associated negative differential conductance. The mechanism leading to this behavior is explained in the previous section. Let us therefore focus now on the behavior of the TMR effect, which is plotted in Fig. 5(c). For a large detuning δ there is, in principle, one transport regime where the sequential tunneling approximation clearly gives an incorrect result for the TMR. This is in the low-bias voltage regime where the sequential processes are suppressed. The total TMR then exhibits a plateau for $E^A_{+-} < eV < E^A_{-+}$ ($-U/2 \lesssim eV \lesssim U/2$), whereas the corresponding $\mathrm{TMR}^{(1)}$, calculated taking into account only the first-order processes, is strongly suppressed. When increasing the bias voltage, $E^A_{-+} < eV < E^A_{++}$ ($U/2 \lesssim eV \lesssim 3U/2$), the current becomes dominated

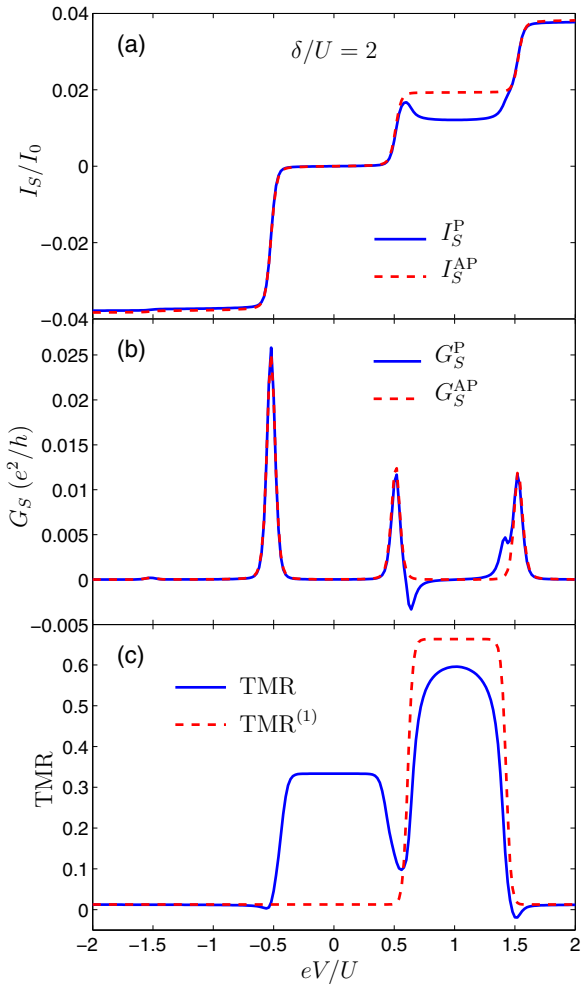

FIG. 5. (Color online) (a) The Andreev current in the parallel (solid line) and antiparallel (dashed line) magnetic configurations, (b) the corresponding differential conductance, and (c) the tunnel magnetoresistance (TMR). For comparison in (c) we also show the TMR calculated using only sequential tunneling processes (dashed line). Parameters are the same as in Fig. 2.

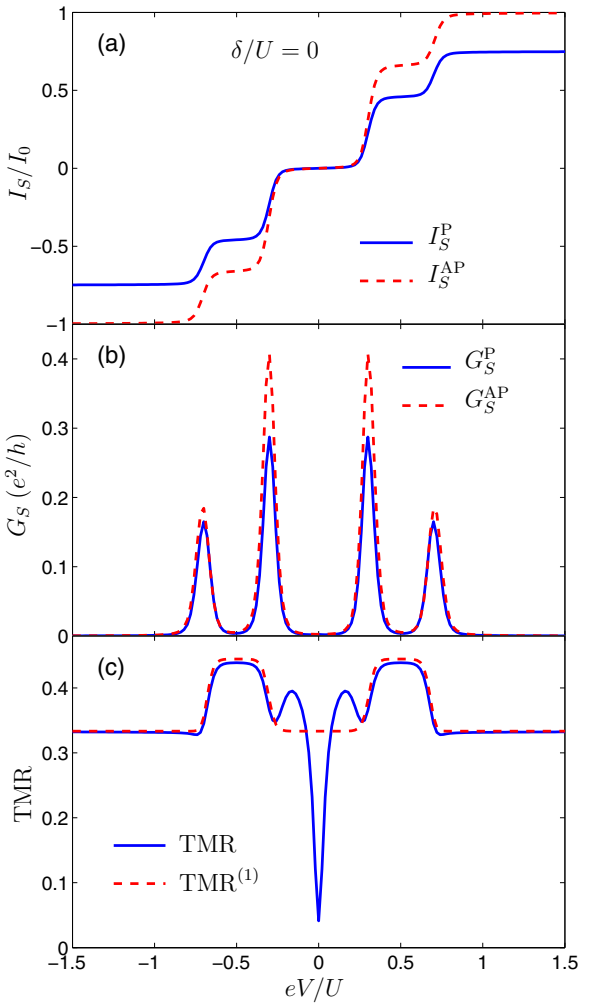

FIG. 6. (Color online) The same as Fig. 5, calculated for detuning $\delta = 0$.

by sequential tunneling, however, second-order processes still lead to a considerable modification of the $\mathrm{TMR}^{(1)}$, namely, to its lowering. On the other hand, for $eV > E^A_{++}$ ($eV \gtrsim 3U/2$) or $eV < E^A_{+-}$ ($eV \lesssim -U/2$), the effect of second-order tunneling on the TMR is rather negligible.

Since TMR exhibits well-defined transport regions where it is constant, one can derive some approximative analytical formulas for the TMR. This can be done by assuming very low temperatures, so that one can replace the Fermi functions with step functions. Then the formula for $\mathrm{TMR}^{(1)}$ calculated for $\delta/U = 2$ describing the value in the plateau ($U/2 \lesssim eV \lesssim 3U/2$) is given by

$$\mathrm{TMR}^{(1)} = \frac{2(1+\varepsilon_A)}{(1+3\varepsilon_A)}\frac{2p^2}{1-p^2}, \tag{12}$$

while the sequential TMR for bias voltages $eV \gtrsim 3U/2$ is given by

$$\mathrm{TMR}^{(1)} = \frac{\varepsilon_A^2 - 1}{2\varepsilon_A^2}\frac{2p^2}{1-p^2}. \tag{13}$$

This analytical expression also describes the TMR for $eV \lesssim -3U/2$. On the other hand, the TMR for $-3U/2 \lesssim eV \lesssim -U/2$ reads

$$\mathrm{TMR}^{(1)} = \frac{2(\varepsilon_A - 1)}{(3\varepsilon_A - 1)}\frac{2p^2}{1-p^2}. \tag{14}$$

Note that the ε_A-dependent ratio in Eq. (12) tends to unity for $\delta = 2U$, whereas the other two factors from Eqs. (13) and (14) approach 0, so that TMR then vanishes. In the Coulomb blockade regime, $-U/2 \lesssim eV \lesssim U/2$, the sequential TMR is clearly wrong because the current is driven by cotunneling processes. To find the formula for TMR in the cotunneling regime, we assume zero temperature and low bias voltage. Moreover, since the dot is in the singlet state, the only relevant cotunneling processes are the spin-conserving ones (elastic processes). Because we are interested in the TMR, which is given by the appropriate ratio of the currents, it is sufficient to consider only the dependence on the couplings to ferromagnetic leads (the denominators of cotunneling rates will cancel). The rate of a cotunneling process is proportional to $\gamma^{\sigma\bar{\sigma}}_{rr'} \sim \Gamma^{\sigma}_{r}\Gamma^{\bar{\sigma}}_{r'}$ and corresponds to transferring the spin-σ electron between the dot and the lead r and the spin-$\bar{\sigma}$ electron

between the dot and lead r'. If $r = r'$, the process is related to direct Andreev tunneling, while for $r \neq r'$ we have a crossed Andreev process. Thus, the current is generally proportional to $I_S \sim \sum_{r,r'=L,R} \Gamma_r^{\sigma} \Gamma_{r'}^{\bar{\sigma}}$, which, with the insertion of the proper coupling constants for a given magnetic configuration, yields

$$I_S^{\mathrm{P}} \sim \Gamma^2(1-p^2) \quad \text{and} \quad I_S^{\mathrm{AP}} \sim \Gamma^2 \tag{15}$$

for the parallel and antiparallel configurations, respectively. The TMR is then given by

$$\mathrm{TMR} = \frac{p^2}{1-p^2}. \tag{16}$$

This formula approximates the TMR in the Coulomb blockade regime when the ground state is a singlet state, which, for assumed spin polarization, gives TMR $= 1/3$ [see Fig. 5(c)].

When the detuning is absent, the Andreev current becomes maximized. This situation is shown in Fig. 6, where the bias dependence of the current, differential conductance, and TMR is presented. First, one can see that the transport characteristics are now symmetric with respect to the bias reversal. The current as a function of the bias voltage changes monotonically, giving rise to four peaks in differential conductance [see Figs. 6(a) and 6(b)]. On the other hand, the TMR out of the Coulomb blockade regime takes well-defined values that can be approximated by considering sequential processes as

$$\mathrm{TMR}^{(1)} = \frac{2}{3}\frac{2p^2}{1-p^2} \tag{17}$$

at the plateau for voltages where the first step in the current occurs as the voltage is increased from $V = 0$, and

$$\mathrm{TMR}^{(1)} = \frac{1}{2}\frac{2p^2}{1-p^2} \tag{18}$$

in the high-voltage regime, $|eV| > E^A_{\pm\pm}$. In the Coulomb blockade regime, $E^A_{-+} < eV < E^A_{+-}$, the dot is singly occupied and the ground state is a doublet. Thus, there are both spin-flip and non-spin-flip cotunneling processes allowed, and providing a simple analytical formula for the TMR in this transport regime is not possible. Moreover, nonequilibrium spin accumulation also builds up in the dot with increasing bias voltage. Altogether this leads to a nontrivial dependence of the TMR on the applied bias, which is clearly different from that predicted within the sequential tunneling approximation [see Fig. 6(c)]. The total TMR has a minimum at the zero bias and then starts to increase with the bias voltage, to drop again just before the threshold for sequential tunneling, giving rise to a local maximum.

Finally, we would like to note that although the analogy to the Julliere model is rather unjustified here, since the considered system is clearly different from a single ferromagnetic tunnel junction, the derived analytical formulas for the TMR can be, oddly enough, expressed in terms of $\mathrm{TMR}^{\mathrm{Jull}} = 2p^2/(1-p^2)$, which is the value characteristic of a ferromagnetic tunnel junction [43].

C. Zero-bias anomaly

The highly nontrivial dependence of the TMR on the bias voltage in the case of $\delta = 0$ [see Fig. 6(c)] suggests that the Andreev conductance must also reveal a nontrivial behavior. This is indeed the case. While in the antiparallel configuration the differential conductance shows a typical parabolic dependence on the applied bias voltage, in the parallel configuration, on the contrary, the differential conductance first drops when the voltage is increased (see Fig. 7). This gives rise to a maximum in the differential conductance in the parallel configuration at zero bias. The maximum bears a strong resemblance to the zero-bias anomaly predicted for quantum dots coupled to ferromagnetic leads, which occurs when the magnetic configuration of the device is antiparallel [44]. Here, in the considered hybrid device, the zero-bias anomaly develops in the parallel configuration and is a direct consequence of the dependence of Andreev processes on the spin polarization of ferromagnets. As shown in the inset in Fig. 7, with increasing bias voltage, nonequilibrium spin accumulation builds up in the dot: the occupation probability of the spin-up level is different from that of the spin-down level. As a consequence, tunneling of Cooper pairs becomes suppressed and the differential conductance drops. With a further increase in the bias voltage, the rate of Andreev processes is enhanced and the conductance starts to increase again, despite the presence of strong nonequilibrium spin accumulation.

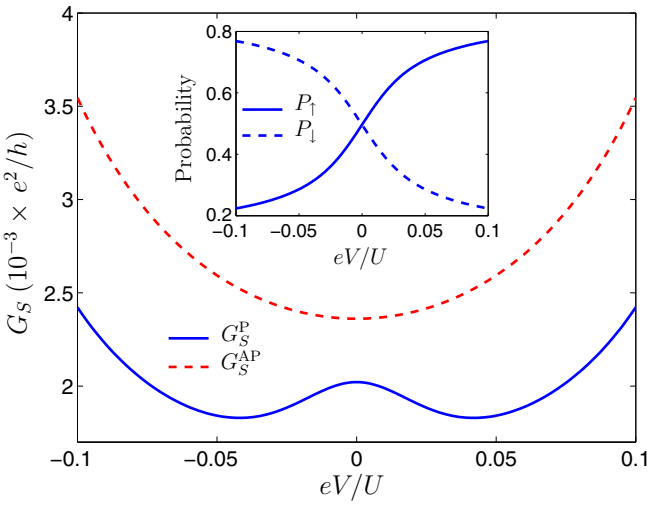

FIG. 7. (Color online) Bias dependence of the Andreev differential conductance for the parallel and antiparallel magnetic configurations calculated for the Coulomb blockade regime with $\delta = 0$. Inset: Relevant occupation probabilities for spin-up and spin-down levels. Parameters are the same as in Fig. 2.

To discuss more specific features of the zero-bias anomaly of the Andreev conductance in the parallel configuration, in Fig. 8 we plot G_S^{P} for different spin polarizations of the ferromagnets, different detunings, and different temperatures. When the spin polarization p is low [see the curve for $p = 0.1$ in Fig. 8(a)], the maximum in G_S^{P} is hardly visible and starts developing only when the spin polarization is increased (see the curves for $p \gtrsim 0.3$). Then, increasing p generally leads to an enhancement of the relative height of the zero-bias anomaly, although the magnitude of the conductance is gradually decreased and should be fully suppressed for $p \to 1$, where it is no longer possible to form a Cooper pair since the

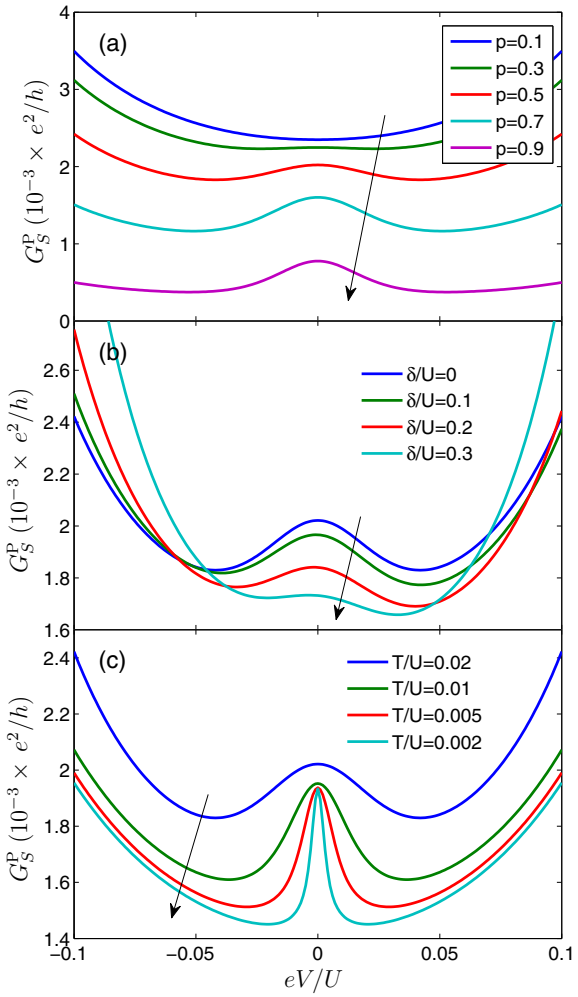

FIG. 8. (Color online) Bias dependence of the Andreev differential conductance in the parallel configuration for different (a) spin polarization p of the ferromagnets, (b) detuning δ, and (c) temperature T. Parameters being changed are specified in each panel, while other parameters are the same as in Fig. 2 with $\delta = 0$. Arrows indicate the direction of change of the parameters that are tuned in each panel.

ferromagnets support only one spin species. The enhancement of the relative height of the peak in G_S^P at zero bias is related to the fact that by increasing p, the nonequilibrium spin accumulation is also increased, which leads to a stronger suppression of the conductance with increasing bias voltage.

The zero-bias anomaly occurs in the Coulomb blockade regime when the dot occupation is odd and it is most pronounced in the case of zero detuning $\delta = 0$. When moving away from the symmetry point, $\delta \neq 0$, the relative height of the maximum in G_S^P is lowered, and for large enough detuning it completely vanishes [see Fig. 8(b)]. This is simply related to the fact that with increasing $|\delta|$, the Coulomb blockade is weakened and the role of the second-order processes is diminished compared to that of the first-order processes. In fact, the role of various second-order processes in the formation of the zero-bias peak can be understood from the bias dependence of G_S^P calculated for different temperatures [see Fig. 8(c)]. It is clearly visible that with decreasing temperature, the width of the zero-bias anomaly is decreased. This dependence is similar to that observed for the zero-bias anomaly, which occurs in the antiparallel configuration for typical quantum dot spin valves [44]. It indicates the role of the single-junction spin-flip cotunneling processes. In the considered three-terminal setup, where the electrochemical potentials of both ferromagnets are kept the same, such spin-flip processes can occur by involving either the two ferromagnetic leads or just a single lead. These processes do not contribute to the Andreev transport, although the Cooper pairs can be created or annihilated in virtual states; however, they can change the dot occupations and thus indirectly affect the current. The rate of such spin-flip processes is proportional to the temperature, $\gamma_{rr'}^{\sigma\bar{\sigma}} \sim \Gamma_r^{\sigma}\Gamma_{r'}^{\bar{\sigma}} T\varepsilon^2/(\varepsilon^2 - \Gamma_S^2/4)^2$. Consequently, with decreasing T the amount of spin flips is reduced, so that the nonequilibrium spin accumulation sets in for lower voltages, and the conductance drop is also shifted towards lower biases. As a result, the width of the zero-bias anomaly becomes linearly reduced with decreasing temperature. In fact, the width of the maximum at zero bias can also provide information about the energy scale at which the transport processes start to dominate over the spin-flip processes. Once this happens, nonequilibrium spin accumulation develops in the dot and G_S^P first drops, to increase further with increasing bias voltage. We also note that at very low temperatures, $T \to 0$, slip-flip processes are not present and the zero-bias anomaly does not develop. The conductance is then due to the processes involving states $|+\rangle$ and $|-\rangle$, whose occupation is low but still finite, giving rise to a finite Andreev current. Nevertheless, in the limit of a very deep Coulomb blockade, $U \gg \Gamma$, the current between the superconductor and the ferromagnetic leads becomes fully suppressed.

IV. CONCLUSIONS

In this paper we have analyzed the Andreev current flowing through a quantum dot connected to one superconducting and two ferromagnetic leads in the sequential and cotunneling regimes. The considerations were based on the real-time diagrammatic technique, which allowed us to systematically study the effect of cotunneling processes on the Andreev current, differential conductance, and resulting TMR. The Andreev current occurs in such a three-terminal setup due to both DAR and CAR. Since upon changing the magnetic configuration of the device, it is CAR which is affected, the role of CAR in transport can be quantified by studying the behavior of the TMR.

We have shown that, depending on the transport regime, the TMR can take well-defined values and can be described by simple analytical formulas. Moreover, we have also shown that the cotunneling processes considerably modify the behavior of TMR in the blockade regions where sequential processes are suppressed. In the blockade regime where the dot ground state is a singlet, the TMR exhibits a plateau with the value given by $p^2/(1 - p^2)$, which is in stark contrast to the highly suppressed TMR obtained within the sequential tunneling approximation. On the other hand, in the Coulomb blockade with a single electron, the TMR exhibits a highly nontrivial dependence on the bias voltage with a minimum at the zero bias, opposite to the sequential TMR, which is constant. This nontrivial dependence

results from a particular dependence of the Andreev current and differential conductance on the applied bias voltage. While in the antiparallel configuration the differential conductance displays a parabolic dependence on the applied bias, in the parallel configuration the conductance exhibits a peak at zero bias. The zero-bias anomaly of the Andreev conductance is related to a nonequilibrium spin accumulation on the dot and a subtle interplay between the spin-flip cotunneling processes that do not contribute to the Andreev current and the processes that drive the current. Since the rate of the former processes depends on the temperature, but that of the latter processes on the applied bias voltage, the width of the zero-bias anomaly strongly depends on the temperature and is decreased with lowering T.

ACKNOWLEDGMENTS

We acknowledge support from Iuventus Plus Project No. IP2011 059471 for the years 2012–2014. I.W. also acknowledges support from EU Grant No. CIG-303 689. P.T. also acknowledges support from the European Union under the European Social Fund Operational Programme Human Capital (POKL.04.01.01-00-133/09-00).

[1] D. D. Awschalom, D. Loss, and N. Samarth (eds.), *Semiconductor Spintronics and Quantum Computation* (Springer, Berlin, 2002).
[2] I. Zutic, J. Fabian, and S. Das Sarma, Rev. Mod. Phys. **76**, 323 (2004).
[3] T. Brandes, Phys. Rep. **408**, 315 (2005).
[4] S. Sahoo, T. Kontos, J. Furer, C. Hoffmann, M. Gräber, A. Cottet, and C. Schönenberger, Nat. Phys. **1**, 99 (2005).
[5] K. Hamaya, M. Kitabatake, K. Shibata, M. Jung, M. Kawamura, S. Ishida, T. Taniyama, K. Hirakawa, Y. Arakawa, and T. Machida, Appl. Phys. Lett. **93**, 222107 (2008).
[6] J. Barnaś and I. Weymann, J. Phys.: Condens. Matter **20**, 423202 (2008).
[7] F. T. Birk and D. Davidović, Phys. Rev. B **81**, 241402(R) (2010).
[8] Sz. Csonka, I. Weymann, and G. Zarand, Nanoscale **4**, 3635 (2012).
[9] A. N. Pasupathy, R. C. Bialczak, J. Martinek, J. E. Grose, L. A. K. Donev, P. L. McEuen, and D. C. Ralph, Science **306**, 86 (2004).
[10] A. Bernand-Mantel, P. Seneor, N. Lidgi, M. Munoz, V. Cros, S. Fusil, K. Bouzehouane, C. Deranlot, A. Vaures, F. Petroff, and A. Fert, Appl. Phys. Lett. **89**, 062502 (2006).
[11] K. Hamaya, S. Masubuchi, M. Kawamura, T. Machida, M. Jung, K. Shibata, K. Hirakawa, T. Taniyama, S. Ishida, and Y. Arakawa, Appl. Phys. Lett. **90**, 053108 (2007).
[12] K. Hamaya, M. Kitabatake, K. Shibata, M. Jung, M. Kawamura, K. Hirakawa, T. Machida, T. Taniyama, S. Ishida, and Y. Arakawa, Appl. Phys. Lett. **91**, 022107 (2007); **91**, 232105 (2007).
[13] K. Hamaya, M. Kitabatake, K. Shibata, M. Jung, M. Kawamura, S. Ishida, T. Taniyama, K. Hirakawa, Y. Arakawa, and T. Machida, Phys. Rev. B **77**, 081302(R) (2008).
[14] H. Yang, S.-H. Yang, and S. S. P. Parkin, Nano Lett. **8**, 340 (2008).
[15] K. Hamaya, M. Kitabatake, K. Shibata, M. Jung, S. Ishida, T. Taniyama, K. Hirakawa, Y. Arakawa, and T. Machida, Phys. Rev. Lett. **102**, 236806 (2009).
[16] M. Gaass, A. K. Hüttel, K. Kang, I. Weymann, J. von Delft, and Ch. Strunk, Phys. Rev. Lett. **107**, 176808 (2011).
[17] W. Rudziński and J. Barnaś, Phys. Rev. B **64**, 085318 (2001).
[18] M. Braun, J. König, and J. Martinek, Phys. Rev. B **70**, 195345 (2004).
[19] A. Cottet, W. Belzig, and C. Bruder, Phys. Rev. Lett. **92**, 206801 (2004).
[20] I. Weymann, J. König, J. Martinek, J. Barnaś, and G. Schön, Phys. Rev. B **72**, 115334 (2005).
[21] L. Hofstetter, A. Geresdi, M. Aagesen, J. Nygård, C. Schönenberger, and S. Csonka, Phys. Rev. Lett. **104**, 246804 (2010).
[22] L. Hofstetter, S. Csonka, J. Nygård, and C. Schönenberger, Nature **461**, 960 (2009).
[23] L. G. Herrmann, F. Portier, P. Roche, A. L. Yeyati, T. Kontos, and C. Strunk, Phys. Rev. Lett. **104**, 026801 (2010).
[24] G. Deutscher and D. Feinberg, Appl. Phys. Lett. **76**, 487 (2000).
[25] D. Beckmann, H. B. Weber, and H. v. Löhneysen, Phys. Rev. Lett. **93**, 197003 (2004).
[26] S. Russo, M. Kroug, T. M. Klapwijk, and A. F. Morpurgo, Phys. Rev. Lett. **95**, 027002 (2005).
[27] J.-F. Feng and S.-J. Xiong, Phys. Rev B **67**, 045316 (2003).
[28] X. F. Cao, Y. Shi, X. Song, S. Zhou, and H. Chen, Phys. Rev B **70**, 235341 (2004).
[29] P. Zhang and Y.-X. Li, J. Phys.: Condens. Matter **21**, 095602 (2009).
[30] K. I. Wysokiński, J. Phys.: Condens. Matter **24**, 335303 (2012).
[31] Y. Zhu, Q.-F. Sun, and T.-H. Lin, Phys. Rev. B **65**, 024516 (2001).
[32] D. S. Golubev and A. D. Zaikin, Phys. Rev. B **76**, 184510 (2007).
[33] D. Futterer, M. Governale, M. G. Pala, and J. König, Phys. Rev. B **79**, 054505 (2009).
[34] B. Sothmann, D. Futterer, M. Governale, and J. König, Phys. Rev. B **82**, 094514 (2010).
[35] H. Schoeller and G. Schön, Phys. Rev. B **50**, 18436 (1994); J. König, J. Schmid, H. Schoeller, and G. Schön, *ibid.* **54**, 16820 (1996).
[36] A. V. Rozhkov and D. P. Arovas, Phys. Rev. B **62**, 6687 (2000).
[37] J. Nagamatsu, N. Nakagawa, T. Muranaka, Y. Zenitani, and J. Akimitsu, Nature **410**, 63 (2001).

[38] B. W. Heinrich, L. Braun, J. I. Pascual, and K. J. Franke, Nature Phys. **9**, 765 (2013).
[39] M. G. Pala, M. Governale, and J. König, New J. Phys. **9**, 278 (2007).
[40] M. Governale, M. G. Pala, and J. König, Phys. Rev. B **77**, 134513 (2008).
[41] I. Weymann, Phys. Rev. B **78**, 045310 (2008).
[42] D. V. Averin and A. A. Odintsov, Phys. Lett. A **140**, 251 (1989); D. V. Averin and Yu. V. Nazarov, Phys. Rev. Lett. **65**, 2446 (1990).
[43] M. Julliere, Phys. Lett. A **54**, 225 (1975).
[44] I. Weymann, J. Barnaś, J. König, J. Martinek, and G. Schön, Phys. Rev. B **72**, 113301 (2005); I. Weymann and J. Barnaś, *ibid.* **75**, 155308 (2007).